

# Early recognition of lung cancer by integrin targeted imaging in K-ras mouse model

Vladimir Ermolayev<sup>1</sup>, Pouyan Mohajerani<sup>1</sup>, Angeliqe Ale<sup>1</sup>, Athanasios Sarantopoulos<sup>1</sup>, Michaela Aichler<sup>2</sup>, Gian Kayser<sup>3</sup>, Axel Walch<sup>2</sup> and Vasilis Ntziachristos<sup>1,4</sup>

<sup>1</sup>Institute for Biological and Medical Imaging, Helmholtz Zentrum Munich, Ingolstaedter Landstrasse 1 D-85764 Neuherberg, Germany

<sup>2</sup>Research Unit Analytical Pathology—Institute of Pathology, Helmholtz Zentrum Munich, Ingolstaedter Landstrasse 1 D-85764 Neuherberg, Germany

<sup>3</sup>Institute of Pathology, Universitätsklinikum Freiburg, Freiburg im Breisgau, Germany

<sup>4</sup>Technische Universitaet Muenchen, Chair for Biological Imaging, Arcisstrasse 21, D-80333, Munich

Non-small cell lung cancer is characterized by slow progression and high heterogeneity of tumors. Integrins play an important role in lung cancer development and metastasis and were suggested as a tumor marker; however their role in anticancer therapy remains controversial. In this work, we demonstrate the potential of integrin-targeted imaging to recognize early lesions in transgenic mouse model of lung cancer based on spontaneous introduction of mutated human gene bearing K-ras mutation. We conducted *ex vivo* and fluorescence molecular tomography-X-ray computed tomography (FMT-XCT) *in vivo* imaging and analysis for specific targeting of early lung lesions and tumors in rodent preclinical model for lung cancer. The lesions and tumors were characterized by histology, immunofluorescence and immunohistochemistry using a panel of cancer markers. *Ex vivo*, the integrin-targeted fluorescent signal significantly differed between wild type lung tissue and K-ras pulmonary lesions (PL) at all ages studied. The panel of immunofluorescence experiments demonstrated that PL, which only partially show cancer cell features were detected by  $\alpha\beta3$ -integrin targeted imaging. Human patient material analysis confirmed the specificity of target localization in different lung cancer types. Most importantly, small tumors in the lungs of 4-week-old animals could be noninvasively detected *in vivo* on the fluorescence channel of FMT-XCT. Our findings demonstrated  $\alpha\beta3$ -integrin targeted fluorescent imaging to specifically detect premalignant pleural lesions in K-ras mice. Integrin targeted imaging may find application areas in preclinical research and clinical practice, such as early lung cancer diagnostics, intraoperative assistance or therapy monitoring.

## Introduction

Non-small cell lung cancer (NSCLC) is the most common type of lung cancer characterized by high heterogeneity including such tumor cell types as adenomas, adenocarcinomas, squamous and large cell carcinomas.<sup>1</sup> NSCLC cells often har-

**Key words:** preclinical cancer models, K-ras, non-small cell lung cancer, fluorescence molecular tomography, X-ray computer tomography, fluorescent contrast agent, integrin

Additional Supporting Information may be found in the online version of this article.

**Grant sponsor:** German Federal Ministry of Education and Science (BMBF); **Grant sponsor:** MOBIMED (Molecular Imaging in Medicine); **Grant sponsor:** MOBITUM (Watching Tumor Biology by Molecular Imaging); **Grant sponsor:** BMBF; **Grant numbers:** 0315508A and 01IB10004E; **Grant sponsor:** Deutsche

Forschungsgemeinschaft; **Grant numbers:** SFB 824 TP B1, SFB 824 TP Z02, WA 1656/3-1

**DOI:** 10.1002/ijc.29372

**History:** Received 17 Jan 2014; Accepted 3 Nov 2014; Online 2 Dec 2014

**Correspondence to:** Prof. Vasilis Ntziachristos, Institute for Biological and Medical Imaging, Helmholtz Zentrum Munich, Ingolstaedter Landstrasse 1 D-85764 Neuherberg, Germany, Tel.: +49(0)89 3187 3852, Fax: +49(0)89 3187 3008, E-mail: v.ntziachristos@tum.de

bor specific mutated oncogene as the primary genetic “driver” leading to cancer. The two most common oncogenes encode for the epidermal growth factor receptor (EGFR) and K-ras.<sup>2</sup> K-ras gene belongs to Rat sarcoma (RAS) gene family regulating cell growth, differentiation and apoptosis by acting within such signaling cascades as mitogen activated protein kinase or phosphoinositide 3-kinase.<sup>3,4</sup> Frequently, NSCLC lung tumorigenesis in mouse models is driven by the activation of K-ras mutations, for example, *K-ras*<sup>LA2</sup> mouse model.<sup>5</sup>

The disease prognosis for NSCLC patients is often dependent on the efficiency of tumor invasion into surrounding tissues, blood vessels and eventually into distant organs.<sup>6</sup> A key factor in the regulation of invasive properties is an integrin mediated adhesive interaction with the surrounding extracellular matrix (ECM). Integrins are heterodimeric adhesive receptors consisting of an  $\alpha$ - and a  $\beta$ -subunit,<sup>7</sup> which control cell movements via dynamic binding to ECM. Alterations in integrin expression, conformational activation and traffic sustain tumor cells with the abnormal ability to cross tissue barriers invading the neighboring organs.<sup>7</sup> Two of the major integrins involved in NSCLC proliferation and metastasis are  $\alpha5\beta1$  and its competitor,  $\alpha\beta3$ , which coordinate the traffic of EGFR, involved in cell proliferation and migration.<sup>8</sup>

$\alpha\beta3$  and  $\alpha5\beta1$  integrins are usually expressed at low or undetectable levels in most adult epithelia but can be highly upregulated in some tumors and angiogenic endothelial cells.<sup>6</sup>

**What's new?**

Integrins play an important role in lung-cancer development and metastasis, and these molecules might therefore be useful as tumor biomarkers. In this study, the authors found that targeted imaging of  $\alpha v \beta 3$ -integrin may allow preclinical researchers and clinicians to detect non-small cell lung cancer (NSCLC) at an earlier stage than accepted cancer markers. This approach may also enhance monitoring of anticancer therapies in early lung cancer.

$\alpha v \beta 3$ -integrin was also initially thought to be involved in pathological angiogenesis due to increased expression in proliferating vascular endothelial cells.<sup>9</sup> As integrin expression in various tumors correlates with disease progression, integrins including  $\alpha v \beta 3$ ,  $\alpha 5 \beta 1$  and  $\alpha v \beta 6$  were suggested as prognostic markers for lung cancer. Further experiments, however, suggested more complicated role for these integrins, for example, antagonists of  $\beta 3$  integrin did not significantly inhibit angiogenesis in clinical trials.<sup>10</sup> Moreover, discrepancies in  $\alpha v \beta 3$ -integrin expression have been reported including both increased and decreased levels in lung adenocarcinoma.<sup>11</sup> The tumorigenic  $\alpha v \beta 3$ -integrin was shown to inhibit tumor progression in mouse models of glioblastoma and melanoma.<sup>12</sup>

Probes targeting  $\alpha v \beta 3$ -integrin were also suggested for cancer imaging and evaluation of antiangiogenic therapies.<sup>13</sup> Coupling M609, an antibody, against  $\alpha v \beta 3$ -integrin, or other antagonists to paramagnetic contrast agents or radionuclides allowed the detection of angiogenic vessels in rabbit and mouse tumor models.<sup>14</sup> Magnetic resonance imaging with  $\alpha v \beta 3$ -integrin-targeted nanoparticle was also used to detect the neovasculature of solid tumors in a xenograft tumor model.<sup>15</sup>  $^{64}\text{Cu}$ -,  $^{18}\text{F}$ - and iron oxide-labeled RGD peptides were used to detect and assess  $\alpha v$  integrins in xenograft models<sup>16,17</sup> and cancer patients.<sup>18</sup>

The great majority of studies concentrated so far on the analysis of developed tumors or tumor metastases, but not in association with the early appearance of the disease. The imaging studies on K-ras mouse models usually involve CT-based assessment in inducible K-ras mutation system and are concentrated on already grown tumors after *Cre-Lox*-mediated activation of tumor development.<sup>19</sup> To our knowledge, there are no systematic studies on the assessment for the potential of integrins, especially tumorigenic  $\alpha v \beta 3$ -integrin as markers for early NSCLC. Besides, due to the discrepancies in integrin localization within lung tumors as well as the weak effects of integrin antagonists in clinical cancer therapy trials, the precise role of  $\alpha v \beta 3$ -integrin in lung cancer remains to be clarified. Within this context, we investigated herein the potential of  $\alpha v \beta 3$ -integrins as early cancer markers. Using optical methods involving a K-ras mouse model of lung cancer,<sup>20</sup> this study also relates to the potential of *in vivo* detection of premalignant and early malignant formations.

**Materials and Methods****Mice and *in vivo* contrast agents**

K-ras transgenic mice (129S/Sv-*Kras*<sup>tm3Tyj/J</sup>), stock number 008185) were purchased from The Jackson Laboratory, Sacramento, CA. Mice homozygous for *K-ras* LA2 allele are lethal. Heterozygote mice develop tumors in the lungs with 100%

incidence, which are first detectable as pleural nodules at one week of age.<sup>20</sup>

Contrast agents, that is, IntegriSense targeting integrin  $\alpha v \beta 3$ ; ProSense activated by Cathepsin B and MMPsense activated by matrix metalloproteinases (MMPs) had excitation and emission peaks at 680 and 700 nm or 750 and 770 nm and were purchased from Perkin Elmer (Waltham, MA). Two nanomoles of each were injected into the tail vein (i.v.) for 4- and 18-week-old animals. Two-week-old animals were injected intraperitoneally (i.p.) due to their small size. The amount of IntegriSense applied was calculated according to the body weight (approximately 0.6 nmol). Twenty-four hours post injection the mice were either anesthetized using isoflurane inhalation and imaged with fluorescence molecular tomography-X-ray computed tomography (FMT-XCT). Alternatively, mice were directly euthanized by Ketamin/Xylazine overdose and whole animals were frozen for slicing-near-infrared-imaging experiment. Following the FMT-XCT imaging, animals were also euthanized and frozen for the sectioning. The animals planned for histological analysis were not frozen, but lungs were excised immediately after euthanasia. Afterwards, they were carefully reinflated by 20% sucrose in phosphate-buffered saline (PBS) and further treated for immunochemistry, or reinflated and incubated overnight in 4% phosphate buffered formaldehyde for preparation of paraffin sections. All mouse handling and experimentation was performed in accordance with German laws and Helmholtz Center and government of Bavaria regulations.

**Slicing and FMT-XCT imaging**

The cryoslicing and imaging experiments were performed at every 250  $\mu\text{m}$  using Multispectral Epi-Illumination Cryoslicing Imaging system as described elsewhere.<sup>21</sup> The *in vivo* hybrid FMT-XCT experiments were performed using the imaging system and method described elsewhere.<sup>22</sup> Briefly, mice were positioned to place thorax region in the camera field of view. FMT scans were obtained every 20° over the full 360° range, resulting in 18 projection angles. At each projection angle, transmission and emission images were acquired for a grid of source positions covering the lung area, using a laser source with the corresponding wavelength (680 or 750 nm). An adaptive algorithm was used to adjust laser power and integration times at each wavelength and source position, as explained elsewhere.<sup>23</sup> The acquired data were then normalized with respect to the applied laser power and integration times to compensate for the differences in these acquisition parameters.

Three-dimensional (3D) XCT volume was obtained using the eXplore Locus micro-CT scanner (GE Healthcare, UK),

as an integrated subsystem of the FMT-XCT system.<sup>23</sup> Acquisition was performed at 400 projections with a rotation step of 0.9°. The tube had energy of 80 kVp and a current of 450  $\mu$ A. The exposure time for each projection was 400 ms. Detector spacing was 29  $\mu$ m and the voxel size was 93  $\mu$ m. The Field of view was 82  $\times$  82 mm in the transverse plane and 43 mm in the axial direction. Filtering was performed to remove low energy photons. No gratings were used.

### Histological analysis

For all histological studies, lungs were excised from the mice. Five-micrometer thick paraffin sections were prepared after lungs were reinflated and incubated overnight in 4% phosphate buffered formaldehyde. Hematoxylin-eosin staining was done as described elsewhere. For immunohistochemistry, excised lungs were carefully re-inflated by 20% sucrose in PBS, incubated in the same solution at 4°C overnight and afterwards inflated with 50% optimal cutting temperature (OCT) compound (Tissue-Tek, Sakura Finetek Europe, Alphen aan den Rijn, The Netherlands) in PBS. Briefly, OCT compound contained about 10% polyvinyl alcohol and 4% polyethylene glycol. Subsequently, lungs were transferred into pure OCT, frozen and cut into 20- $\mu$ m-thick sections. Immunohistochemistry was performed on frozen sections by using antibodies against: Cathepsin B (Santa Cruz Biotechnology, Heidelberg, Germany), E-Cadherin (Cell Signaling Technology, Danvers, MA), macrophages (Mac 3, BP Biosciences, Heidelberg, Germany), EGFR (Cell Signaling Technology, Danvers, MA), Thyroid Transcription Factor-1 (Thermo Fisher Scientific, Bonn, Germany), EphA2 (Abcam, Cambridge, UK), Ki-67 (Abcam, Cambridge, UK), SP-C (Santa Cruz Biotechnology, Heidelberg, Germany) and  $\alpha$ v $\beta$ 3 integrin (Abcam, Cambridge, UK) antibodies. The reaction was visualized with Alexa 594- or Alexa 488-conjugated secondary antibody (Invitrogen, Darmstadt, Germany). Adjacent sections with similar treatment, but with omitted primary antibody provided negative controls. Images were captured with Leica fluorescent microscope (Leica Microsystems, Wetzlar, Germany).

Immunohistochemical staining and analysis of human patient material was performed on tissue microarrays (TMA) using a Discovery XT automated staining platform (Ventana, Tucson, AZ). All tissue specimens analyzed in this study were obtained from patients at Universitaetsklinikum Freiburg, Germany, who gave their written informed consent. This study was approved by the Ethics Committee of the Universitaetsklinikum Freiburg. The patient data included the information on TNM cancer staging and age for each patient. Rabbit anti-integrin alpha v (anti-ITGAV, Atlas Antibodies, Stockholm, Sweden) at a dilution of 1:500 (0.1  $\mu$ g/ $\mu$ L) was used as primary antibody. Secondary antibody was Discovery TM Universal (Ventana). Signal detection was performed using peroxidase-DAB (diaminobenzidine)-MAP kit (Roche, Ventana, Tucson, AZ). Tumors were considered as positive for integrin alpha v when at least 50 % of tumor cells showing a positive pronounced membrane staining.

### Image evaluation and quantification

The *ex vivo* stacks of fluorescence and color images obtained from cryosections were quantified in the Fiji (ImageJ) software (<http://fiji.sc/Fiji>). All the stacks were quantified in original form. Three to five regions of interest (ROI) of identical size were taken for each tissue. ROIs in lung parenchyma tissue outside large blood vessels for wild type (WT), lesions (2-week-old mice) or tumors (4- and 8-week-old mice) for K-ras mice were analyzed along with heart, spinal cord or skin in the vicinity of lungs (Fig. 4a). When no visible lesions could be found, the corresponding lung tissue outside large blood vessels was taken into analysis. Three to five sections were analyzed for each mouse. Fluorescence mean values were transferred to Microsoft Excel (Microsoft Deutschland GmbH, Unterschleissheim, Germany) and the ratios of lung/lesion/tumor versus spinal cord, heart and skin in appropriate ROIs were calculated for each section. Statistical analysis and comparison of different experimental groups using non-paired *t*-test was implemented using GraphPad Prism Software (GraphPad Software La Jolla, CA). To reconstruct XCT and FMT-XCT images, we used an proprietary software developed in our institute for processing hybrid FMT data in MATLAB software package (MathWorks, Ismaning, Germany) environment [PLEASE CITE MY THESIS: Mohajeri, P. (2014). "Robust methods and algorithms for fluorescence imaging and tomography" (Doctoral dissertation, Universitätsbibliothek der TU München)]. The background subtraction was performed to reduce the effect of nonspecific probe accumulation, The mathematical grounds of the background subtraction method were previously described.<sup>24</sup> Briefly, the method used the fact that homogenous background signal contributed an additional term to the measured Born ratio.<sup>25</sup> This additional term constituted a linear function of the source-detector spatial distance. Accordingly, after the measurements, a linear estimation was performed to subtract this term and hence, compensate for the background signal. Specific details of our implementation of this background subtraction approach were explained elsewhere.<sup>26</sup> Amira software (Visage Imaging, Berlin, Germany) was used for 3D visualization of the reconstructed images. All FMT-XCT images presented in this work used exactly the same set of processing parameters in the forward and inverse modeling parts, such as background subtraction parameters, number of inversion iterations and signal thresholds.

### Results

Examination of  $\alpha$ v $\beta$ 3-integrin as a potent imaging marker for lung cancer was performed using a mouse model based on somatic activation of the K-ras oncogene based on spontaneous recombination events causing the early onset of lung cancer after the first week of age with 100% incidence in the lung.<sup>20</sup> We concentrated on the tumor markers showing potential for *in vivo* imaging and cancer detection with special emphasis on the early recognition of lung lesions and

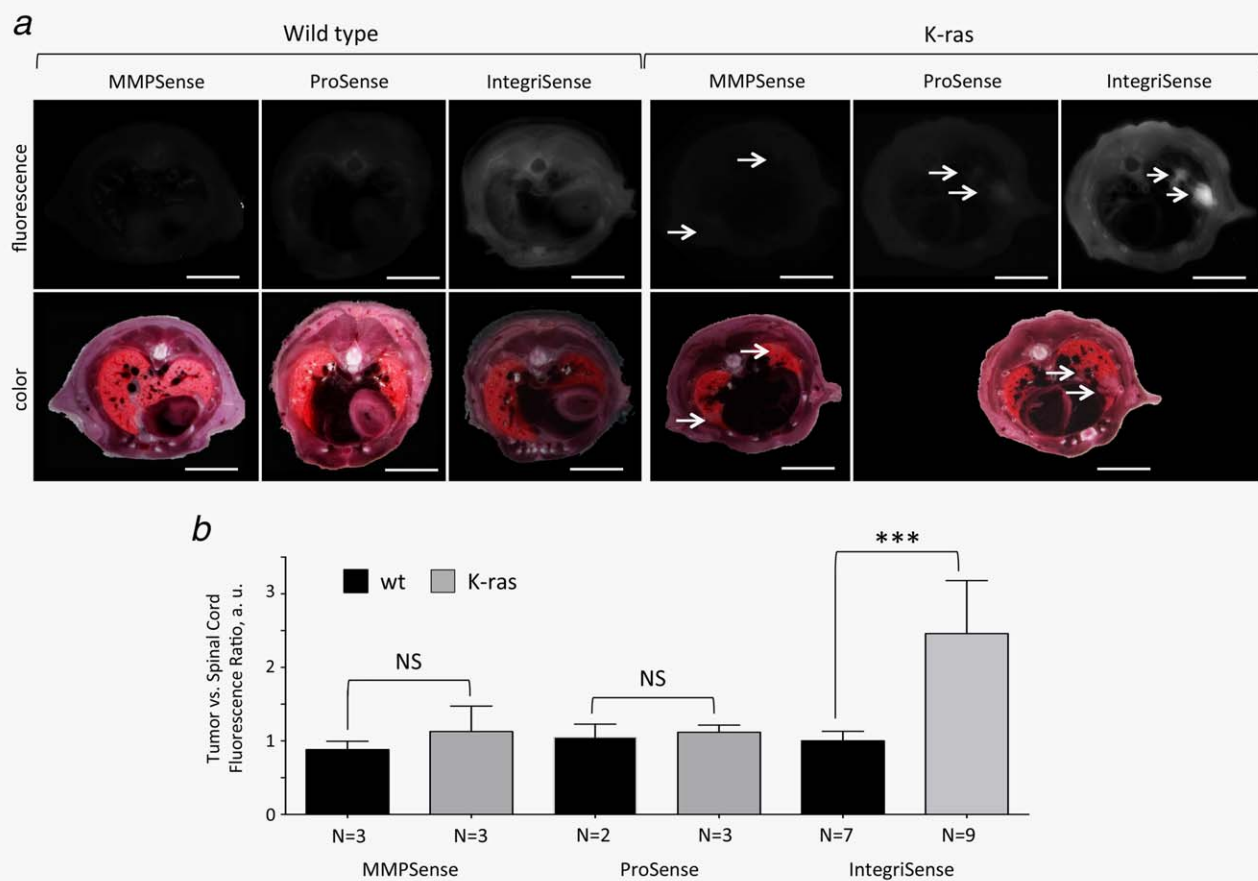


**Figure 1.** Integrin-targeting contrast agent IntegriSense demonstrated the best specific fluorescence accumulation in the tumors inside K-ras lungs from 18-week-old mice versus ProSense and MMP-Sense probes as detected on transversal whole-mouse frozen sections. A. Showing comparable performance in the WT lungs, IntegriSense accumulated more specifically in the lung tumors (arrows) of K-ras mice as compared to the other agents. B. The fluorescence signal for ProSense, MMP-Sense and IntegriSense was calculated in the lungs of 18-week-old WT and K-ras mice (5 sections each) as a signal ratio to spinal cord reference area on the same slice and normalized to WT. Only IntegriSense demonstrated the signal level significantly different from the WT. The differences between experimental groups were analyzed using nonpaired *t*-test. In total, 15 (10) sections and 130 (100) ROIs were analyzed for K-ras (WT) mice injected with MMP-Sense; 14 (14) sections and 120 (140) ROIs were analyzed for K-ras (WT) mice injected with ProSense; 45 (27) sections and 394 (216) ROIs were analyzed for K-ras (WT) mice injected with IntegriSense. \*\*\* -  $p = 0.0002$ . NS – non significant. N – quantity of analyzed animals. [Color figure can be viewed in the online issue, which is available at [wileyonlinelibrary.com](http://wileyonlinelibrary.com).]

tumors.  $\alpha v\beta 3$ -integrin visualization using IntegriSense, a targeted nonpeptidic fluorescent molecule, was contrasted to the ProSense and the MMP-Sense protease activated agents. ProSense sensitive to cathepsins is implicated in tumor growth and was successfully used for imaging in a Lewis Lung Carcinoma model.<sup>27</sup> MMP-Sense is activated by MMPs and is involved in tumor cell invasion and adenocarcinoma development in patients with NSCLC.<sup>28</sup>

#### Selective accumulation of IntegriSense in pleural lesions and tumors

Initially, we studied the accumulation of all agents in the lungs of adult mice (18 weeks of age). As demonstrated in Figure 1, IntegriSense showed comparable performance in the WT lungs, but superior tumor accumulation and specificity for pleural lesions and tumors of K-ras animals as compared to ProSense and MMP-Sense (Fig. 1a). To achieve the

highest possible precision in fluorescence assessment, ProSense, MMP-Sense and IntegriSense signal levels were calculated in the lungs of adult WT and K-ras mice as a signal ratio to spinal cord reference area and normalized to the WT. As only IntegriSense demonstrated fluorescence in lesions/tumors significantly enhanced compared to the WT lung parenchyma (Fig. 1b,  $p = 0.0002$ ), it was chosen for the next experiments. Accumulation of IntegriSense was further assessed in mouse lungs at three different ages: 2, 4 and 18 weeks. No tumors or tissues specifically accumulating IntegriSense could be found in the lungs of WT animals at any age (Fig. 2a, WT). Specific IntegriSense signal was observed in tumors of 4- and 18-week-old mice, the older showing greater number of larger IntegriSense-positive tumors. The rest of lungs including blood vessels, airways and lung parenchyma showed much lower fluorescence signal (Fig. 2a and Supporting Information Fig. 1).

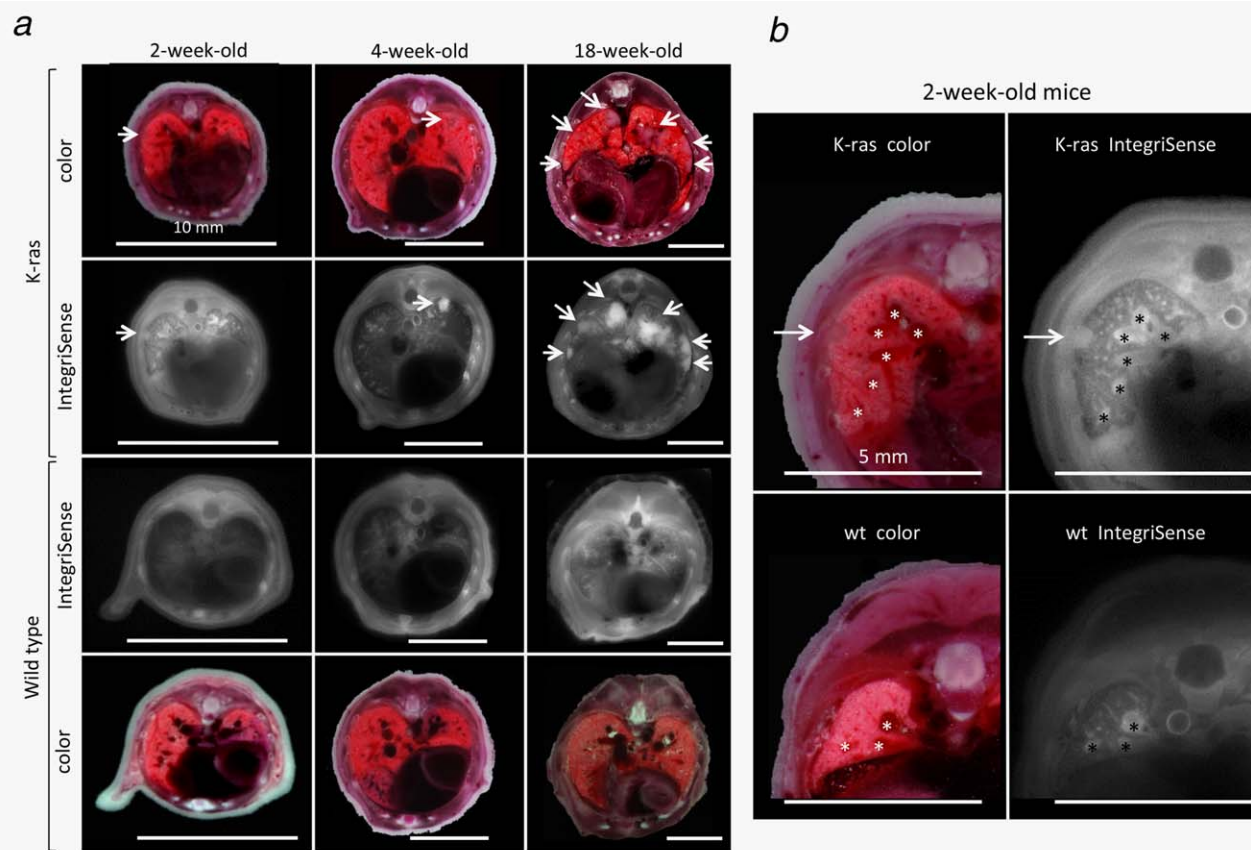


**Figure 2.** *Ex vivo* imaging demonstrated IntegriSense accumulation in PL/tumors at 2, 4 and 18 weeks of age. **A.** IntegriSense-positive PL/tumors of 2-, 4- and 18-week-old K-ras mice (arrows) corresponded well to the ones appearing on the color images from the same cryosections. The lesions/tumors demonstrated similar shape throughout all ages studied distinct from lung parenchyma as well as PBVA. Such lesions or tumors were never detected in WT littermates. **B.** IntegriSense-positive pleural lesions (arrows) were observed in the lung periphery of 2-week-old K-ras, but not WT mice. IntegriSense was also intensively accumulated in developing PBVA (asterisks), however their morphology and localization pattern were clearly distinct from pleural lesions both on fluorescence and corresponding color images. IntegriSense accumulation in the PBVA at 2 weeks of age was complicating the lesion detection. The minimal detectable diameter of a pleural lesion could be assessed for 2-week-old animals as 200 $\mu$ m. [Color figure can be viewed in the online issue, which is available at [wileyonlinelibrary.com](http://wileyonlinelibrary.com).]

At 2 weeks of age, IntegriSense was detected in pleural lesions, however, large blood vessels and airways also showed relatively high accumulation (Fig. 2). The lungs of 2-week-old mice K-ras and WT littermates were compared to better understand the distribution of IntegriSense. Figure 2b shows IntegriSense-accumulation in pleural lesions of the lung periphery at 2 weeks of age, but also in structures corresponding to pulmonary blood vessels and airways (PBVA), IntegriSense-positive PBVA regions are easily visible on comparison of fluorescence and color images from the same cryosection (Fig. 2b, asterisks), but also displayed high variability (Supporting Information Fig. 2). The lesions of 200  $\mu$ m minimal size could be distinguished from lung parenchyma due to characteristic form and preferential localization in the lung periphery, which correlated with previous data.<sup>20</sup> Despite accumulation in lesions at early stage of tumor development, though, IntegriSense did not show enough tumor specificity at this stage since PBVA demonstrated variable, but comparable or sometimes even more intense fluorescence than in lesions.

Lesions were observed in the majority of 2-week old K-ras (out of total nine mice studied, in one pleural lesions were not observed), but never in wild-type littermates. Color and form as well as histological hallmarks of IntegriSense-positive lesions were similar to developed lung tumors, but differed from PBVA regions (Fig. 2b and Supporting Information Fig. 1). Similar pleural lesions were previously described in K-ras mouse model as closely resembling 'atypical adenomatous hyperplasia', precursor to lung carcinoma.<sup>20</sup>

#### Quantitative evaluation of IntegriSense fluorescence

To precisely assess the capacity of integrin targeting for pre-clinical and, possibly, clinical diagnostic imaging, we performed quantitative evaluation of IntegriSense accumulation versus different reference areas obtained by *ex vivo* cryoslicing imaging. The fluorescence in the ROI within lesions/tumors was quantified as a ratio versus (*vs.*) background from different reference areas. The comparison versus spinal cord, skin and heart was performed to evaluate IntegriSense

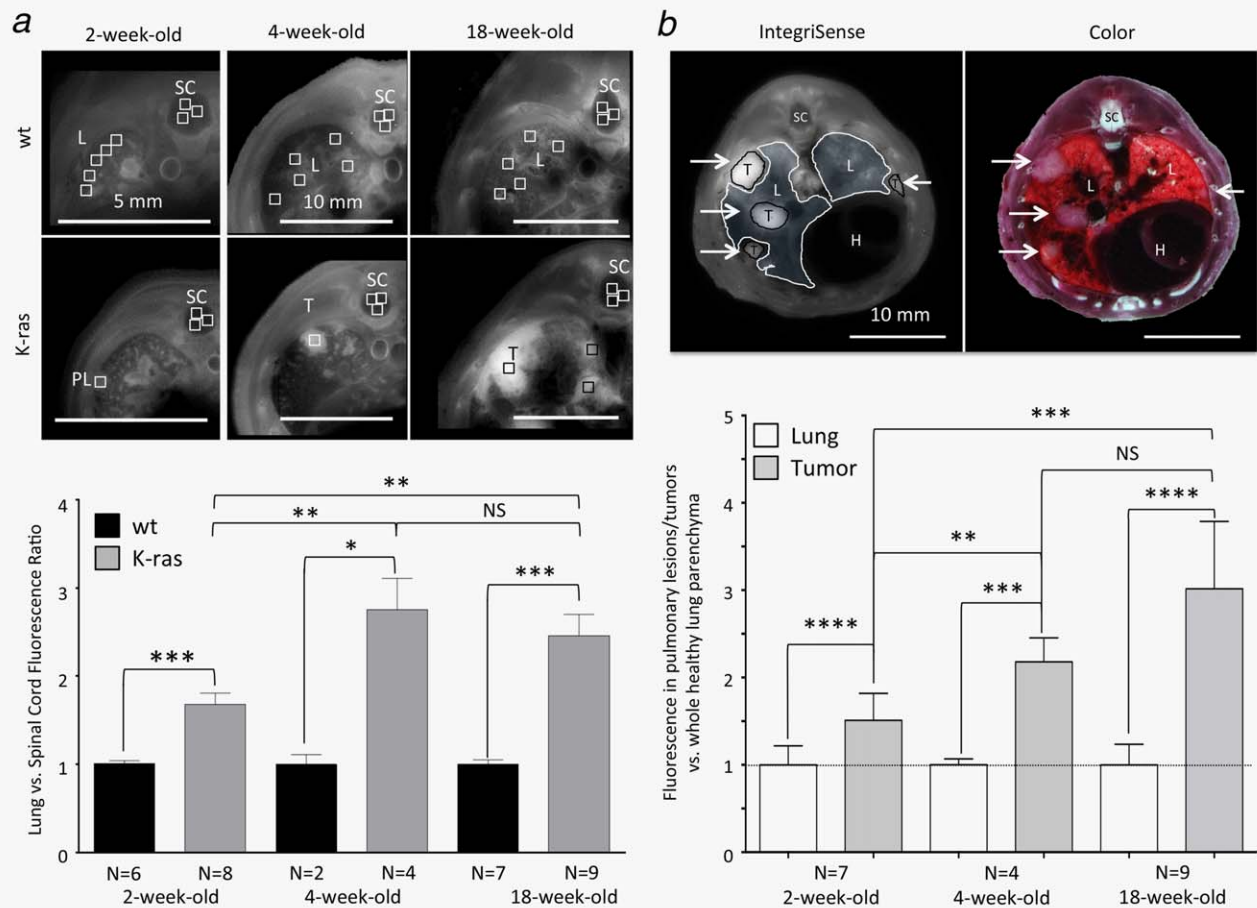


**Figure 3.** Analysis of IntegriSense distribution revealed significantly enhanced fluorescence signal in PL and tumors from K-ras mice versus WT and K-ras lung parenchyma. **A.** IntegriSense fluorescence was calculated as a signal ratio versus background fluorescence in spinal cord (SC) as internal reference area. The fluorescence signals were analyzed in the ROIs on the images from transversal whole mouse frozen sections. Upper panel: representative images showing ROI location. PL – pleural lesion; T – tumor; SC – spinal cord as a reference area. L – lung parenchyma. Lower panel: fluorescence signal ratios were normalized to mean fluorescence of WT lungs. IntegriSense accumulation significantly differed between WT and K-ras littermates for all ages studied. IntegriSense fluorescence was also significantly enhanced in tumors of 4- as well as 18-week-old versus lesions from 2-week-old K-ras animals. In total, 45 (27) sections and 197 (108) ROIs were analyzed for 18-week-old K-ras (WT) mice; 13 (10) sections and 52 (40) ROIs for 4-week-old K-ras (WT) mice; 32 (25) sections and 116 (85) ROIs for 2-week-old K-ras (WT) mice. \*\*\* -  $p \leq 0.0001$ , \*\* -  $p = 0.0072$ , \* -  $p = 0.0151$ . **B.** K-ras experimental group was also tested for the quantitative contrast between IntegriSense accumulation in pleural lesions or tumors (T) versus healthy lung parenchyma (L). Upper panel: Mean fluorescence was quantified in ROIs from lesions/tumors and whole healthy lung parenchyma, as shown on 18-week-old mouse section as an example. Arrows: tumors. H – heart, SC - spinal cord. Lower panel: IntegriSense signal shows enhanced accumulation in the lesions/tumors as compared to the lung parenchyma level (dashed line). Adult lungs show significantly enhanced contrast compared to 2-week-old ones. This analysis was performed on 36 sections and 128 ROIs for 18-week-old K-ras mice; 16 sections and 62 ROIs for 4-week-old ones; 23 sections and 81 ROIs for 2-week-old ones. \*\*\*\* -  $p < 0.0001$ , \*\*\* -  $p = 0.0002$ . \*\* -  $p = 0.0061$ . The differences between experimental groups were analyzed using nonpaired *t*-test. NS – non significant. N – quantity of analyzed animals. [Color figure can be viewed in the online issue, which is available at [wileyonlinelibrary.com](http://wileyonlinelibrary.com).]

contrast to the WT lungs as an early primary diagnostic tool. As shown on Figure 3a, due to reported peripheral location of lesions in 2-week-old mice,<sup>20</sup> ROIs in WT lungs were positioned in the lung periphery out of large PBVA. In adult animals, ROIs were positioned in different lung areas to possibly assess the majority of lung parenchyma. Lower panel on Figure 3a shows that pulmonary lesions (PL) and tumors accumulated significantly higher IntegriSense fluorescence than corresponding WT areas. 1.68-fold higher fluorescence was accumulated in pleural lesions of 2-week-old K-ras mice

compared to WT. 2.76-fold and 2.46-fold enhancement observed for 4-week-old and 18-week-old animals, respectively. Highly significant differences were demonstrated in K-ras versus WT littermates for 2- and 18-week-old mice ( $p < 0.0001$ ). Significant differences were found between lesions/tumors in 2- and 4-week-old as well as 2- and 18-week-old K-ras animals ( $p = 0.0072$ ), nonsignificant between 4- and 18-week-old ones (Fig. 4b). It has to be noted that PBVA fluorescence was enhanced about 1.5-fold versus spinal cord reference area, but displayed very high variability and

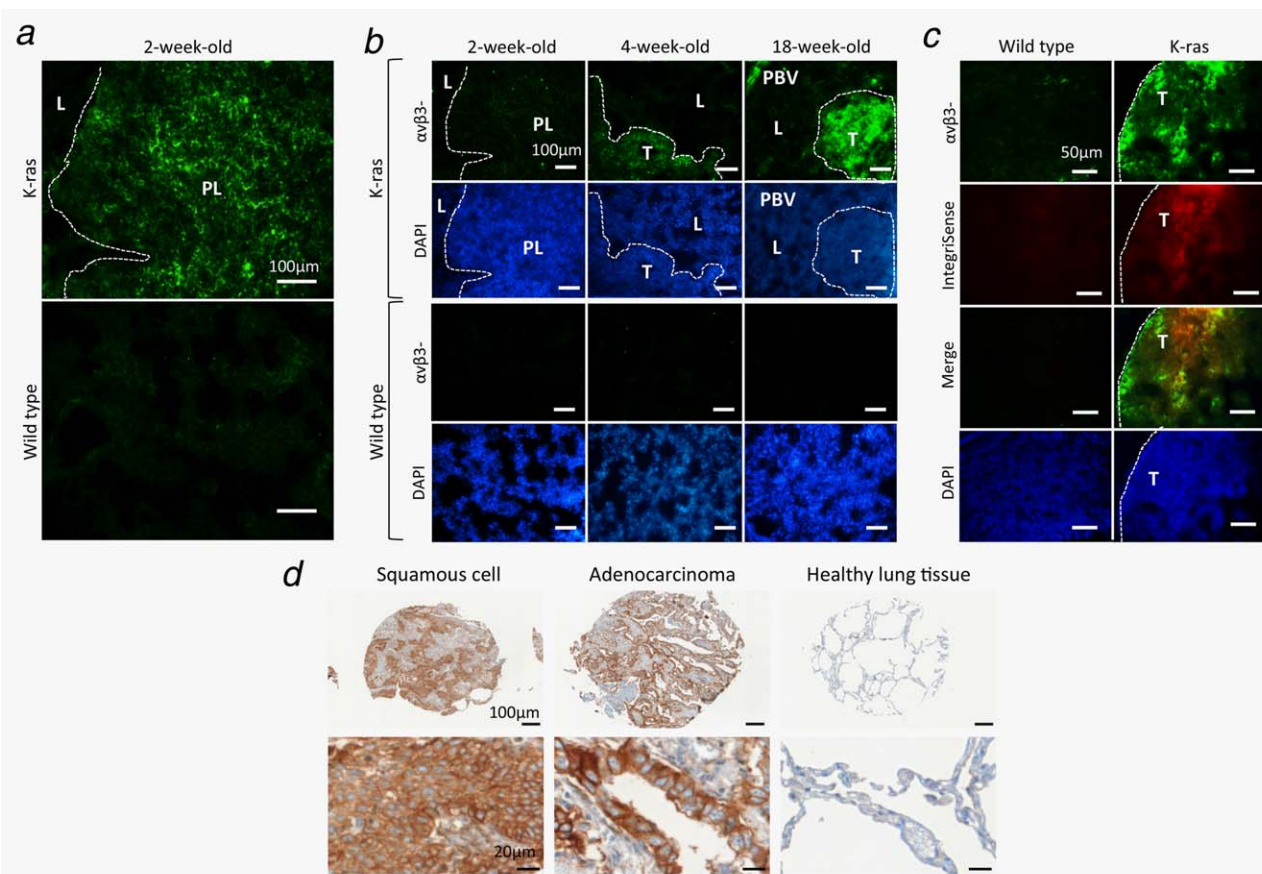


**Figure 4.** Localization of IntegrinSense and integrin target in mouse and human lungs. A. Enhanced accumulation of  $\alpha\text{v}\beta_3$ -integrin could be clearly observed in the pleural lesion (PL) or tumor (T) area from isolated lungs of 2 week old K-ras mice, but not in healthy lung parenchyma (L) from both K-ras and WT animals. PBV – pulmonary blood vessel. B.  $\alpha\text{v}\beta_3$ -integrin accumulation level was enhanced from 2-week-old to 4- and 18-week-old mice. All the images were done within one immunofluorescence experiment, taken under exactly same conditions, combined and contrasted as one image. The images from  $\alpha\text{v}\beta_3$ -integrin staining from 2-week-old mice are the same as on A, but differently contrasted. C. Colocalization of IntegrinSense and  $\alpha\text{v}\beta_3$ -integrin in the lung tumor region on the whole mouse cryosections from 18-week-old K-ras mice. Merged image is shown by yellow-orange colors, where  $\alpha\text{v}\beta_3$ -integrin (green) and IntegrinSense (red) colocalize. The slides were analyzed in the same way as in A and B. B and C. Nuclear counter-stain DAPI performed on the same sections served as a tissue control. Dashed line shows the lesion/tumor margins. C. Representative images for  $\alpha\text{v}$ -integrin localization in patient tumor versus healthy lung TMA. The  $\alpha\text{v}$ -integrin stain is shown in brown. [Color figure can be viewed in the online issue, which is available at [wileyonlinelibrary.com](http://wileyonlinelibrary.com).]

therefore this enhancement could not be significantly distinguished from WT (Supporting Information Fig. 2). IntegrinSense fluorescence was also significantly enhanced in lesions/tumors versus other background tissues, that is, heart and skin, at all animal ages including premalignant lesions in 2-week-old mice (Supporting Information Figs. 3 and 4).

Another analysis was performed to study IntegrinSense accumulation versus healthy lung parenchyma in the same K-ras animals (Fig. 3b). Such analysis demonstrated the capacity of integrin-targeted imaging as a tool to detect different tumors on the background of lung tissue at different disease stages. Median value of the fluorescence signal in the whole tumors was compared to fluorescence in the whole healthy lung parenchyma. Lower panel on Figure 3b shows the analysis summary, which reveals IntegrinSense having higher accumulation in the lesions than in surrounding lung tissue already at 2 weeks of age ( $1.51 \pm 0.31$ -fold higher than

lung parenchyma with high significance degree,  $p < 0.0001$ ). Adult animals showed significantly enhanced contrast ( $p = 0.0061$  for 2- vs. 4-week-old and  $p = 0.0002$  for 2- vs. 18-week-old mice), which, in turn, was not significantly different between 4- and 18-week-old animals ( $2.22 \pm 0.27$ -fold and  $2.81 \pm 0.77$ -fold enhancement). Similar analysis using multiple identical ROIs inside tumor and throughout the whole healthy lung parenchyma revealed very similar results to the ones with variable ROIs, which were reported above (Supporting Information Fig. 5).

#### Specificity of IntegrinSense binding: Assessment in preclinical model and patients

The specificity of IntegrinSense for *in vivo* targeting was confirmed by colocalization of IntegrinSense and its target in mouse lungs.  $\alpha\text{v}\beta_3$ -integrin level detected by immunofluorescence was enhanced in the PL as compared to healthy

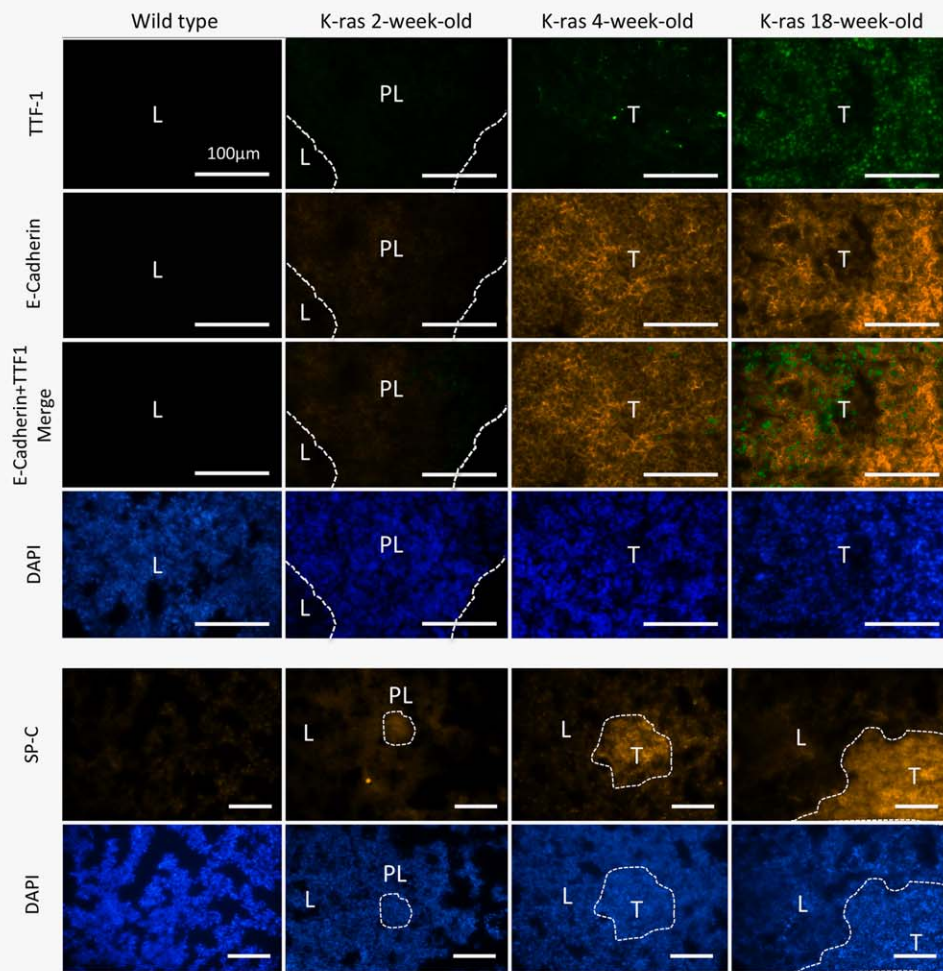


**Figure 5.** The levels of different cancer markers increase in the lesions/tumors from 2- to 4- and 18-week-old mice, and is the lowest in the lungs of WT littermates. TTF-1 and E-Cadherin colocalization is the marker for adenocarcinoma. SP-C is the marker for adenoma. All marker levels were identical between lung parenchyma from all WT mice and therefore the images from 4-week-old mice were taken as representative ones. Nuclear counter-stain DAPI performed on the same sections served as a tissue control. All the images were developed and acquired within one immunofluorescence experiment under exactly the same conditions, combined and contrasted as one image. Dashed line shows the lesion/tumor margins. L – lung parenchyma; PL – pulmonary lesion; T – tumor. [Color figure can be viewed in the online issue, which is available at [wileyonlinelibrary.com](http://wileyonlinelibrary.com).]

lung parenchyma (L) in K-ras and WT animals already at 2 weeks of age (Fig. 4a) and further elevated in tumors (T) at 4- and 18 weeks (Fig. 4b). This result correlated with IntegriSense signal elevation observed macroscopically (Fig. 2). IntegriSense also directly colocalized with  $\alpha v\beta 3$ -integrin staining in tumors of K-ras mice, but not in the other lung tissue or in WT mice (Fig. 4b). In order to assess the accuracy of the lesion/tumor detection by IntegriSense fluorescence compared to the analysis of color images, we performed macroscopic analysis of *ex vivo* image stacks. In the majority of cases, analysis of IntegriSense profile allowed better detection of tumors (Supporting Information Fig. 6), however the evaluation of both color and fluorescence profiles proved to be the best way for reliable tumor detection and discrimination from possible false positives, especially in case of small tumors. This analysis further

confirms the importance of integrin targeting and may present a basis for possible recommendations at clinical applications.

IntegriSense was developed as an agent for *in vivo* detection and quantification of  $\alpha v\beta 3/\alpha v\beta 5$  integrins with preference to  $\alpha v\beta 3$ .<sup>29</sup> Therefore, the applicability of IntegriSense-assisted imaging in clinic was assessed by  $\alpha v$ -integrin assay on human lung cancer TMA. IntegriSense target was recognized in 76.4% patients with squamous cell carcinoma ( $n = 89$ ) and in 68.9% patients with adenocarcinoma ( $n = 45$ ) with no positivity in the healthy lung tissue ( $n = 78$ , Fig. 4c). The additional analysis was also performed using the data on patient age and TNM cancer staging. Such study revealed no significant correlation between the level of  $\alpha v$ -expression and disease staging or age of patients (data not shown).

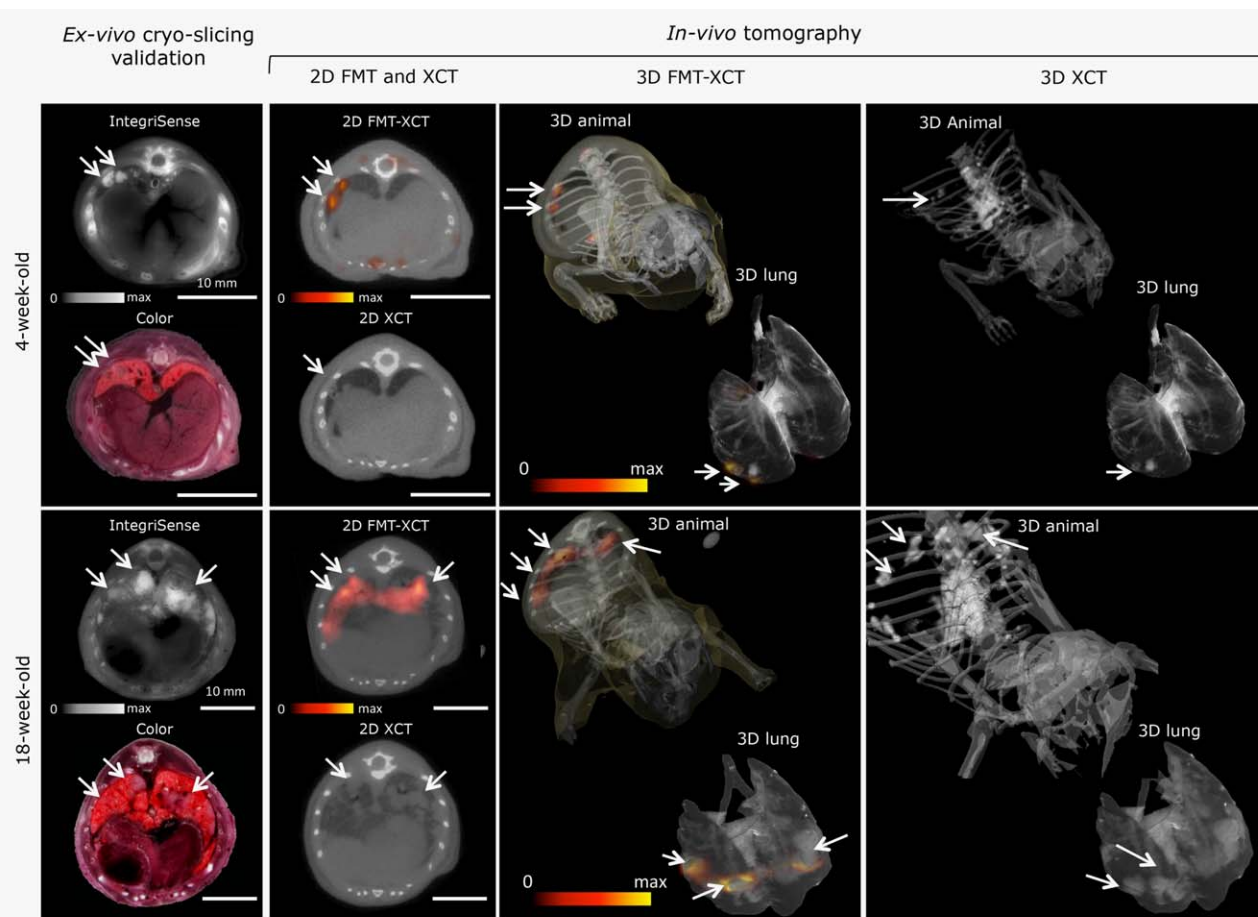


**Figure 6.** FMT-XCT *in vivo* imaging of the thorax area from K-ras mice enables robust detection of lung tumors starting from 4 weeks of age. The 2D and 3D FMT-XCT images were compared with corresponding XCT ones and validated versus *ex vivo* fluorescence and color images from cryosections. The FMT signal enabled specific recognition of tumors on both 3D reconstructions of thorax area of the whole mouse (3D animal) or 3D rendering of lungs only (3D lung), which detection was sometimes problematic by using XCT contrast only. The color scales represent relative intensity of IntegriSense fluorescence signal in arbitrary units. Arrows: detectable tumor areas. [Color figure can be viewed in the online issue, which is available at [wileyonlinelibrary.com](http://wileyonlinelibrary.com).]

### Cancer marker localization in WT and K-ras mouse lungs

For further characterization of pleural lesions and tumors, we performed immunolocalization studies for panel of different cancer-relevant markers. Distribution of adenocarcinoma markers, Thyroid Transcription Factor 1 (TTF-1) and E-Cadherin<sup>30</sup>; and alveolar adenoma marker, surfactant apoprotein-C (SP-C)<sup>27</sup> was studied to test the hallmarks of major cancer types. The majority of lesions/tumors showed TTF1+E-Cadherin staining proving the adenocarcinoma cell type (Fig. 5). Minority of the lesions or foci in the existing ones were SP-C-positive for adenoma. Heterogenic nature of tumors was already reported for NSCLC<sup>1</sup> and particularly for this mouse model.<sup>20</sup> Enhanced TTF1+E-Cadherin and SP-C could be localized already in the PL at 2 weeks of age (Supporting Information Fig. 7) and was further elevated in tumors at four reaching maximum at 18 weeks (Fig. 5).

The markers connected with NSCLC progression and cell proliferation, such as EGFR<sup>31</sup>, tyrosine kinase receptor EphA2<sup>32</sup> and Ki-67<sup>33</sup> were also analyzed. EGFR level was

enhanced versus WT in the lesions of 2-week-old and further elevated for 4- and 18-week-old mice. EphA2 level was comparable to WT in 2-week-, but was enhanced for 4- and 18-week-old mice. Ki-67 immunofluorescence was slightly elevated versus WT in 2- and 4-week-old mice, and was clearly higher in tumors at 18 weeks. (Supporting Information Fig. 8). Taken together, the immunolocalization study combined with histological hallmarks (Supporting Information Fig. 1) implies lesion cells at 2 weeks started malignant transformation, but did not show critical features of developed tumors as for 4- and 18-week-old mice.

### *In vivo* imaging of integrin fluorescence and tumor detection in 3D models

The potential of the IntegriSense for noninvasive *in vivo* imaging was explored by applying FMT-XCT for IntegriSense distribution analysis in 2-, 4- and 18-week-old mice. The reconstruction of IntegriSense spatial distribution proved to be very complicated for 2-week-old mice due to small size of

animals, high background fluorescence and variability of agent accumulation in the PBVA (Supporting Information Fig. 2). *In vivo* spatial analysis and 3D map of IntegriSense distribution could be successfully performed for 18-week-old and also, after background subtraction, for 4-week-old mice despite lower agent accumulation in tumors (Fig. 6). Comparison between nonspecific XCT and integrin-positive FMT-XCT in 2D and 3D revealed the capacity of this imaging modality for robust tumor detection. Especially small tumors were hard to detect on XCT images without specific contrast. The in-depth analysis and comparison of 2D FMT-XCT and XCT stacks, however, demonstrated some limitations of this *in vivo* imaging method. The FMT-XCT imaging was not completely free of false positive results, the majority of which however could be attributed to the artifacts out of lung area. Due to the use of prior XCT-based information in the FMT-XCT reconstruction, such artifacts along with the false positive signals from ribs could be discarded (Supporting Information Fig. 9). Another possible problem could be the difficulty to detect all the tumors at very massive tumor burden that is why the combination of FMT and XCT channel information could be considered as significantly more reliable than one of the channels alone (Supporting Information Fig. 10). Rendered 3D lung models additionally demonstrated the superior performance of FMT specific contrast versus XCT model for the tumor detection (Fig. 6). Finally, the comparison between *in vivo* data from K-ras and WT littermates clearly demonstrates that FMT-XCT detection clearly discriminates between tumor burden in K-ras and heterogeneous lung structure in WT mice, which is far less obvious using merely XCT contrast (Supporting Information Fig. 11). 3D rendering of *ex vivo* cryoslicing image stacks from thorax area of K-ras mice also showed importance of IntegriSense specific contrast for tumor detection versus color imaging (Supporting Information Fig. 12). The 3D reconstructions of organs and whole body regions stressed the importance of the specific contrast information for reliable noninvasive tumor detection.

## Discussion

The efforts in the cancer research community to explore cancer markers relevant for diagnostic and therapy monitoring yield agents based on developed tumor hallmarks or tissue examination post mortem. This approach does not always reveal correct insights into tumor progression *in vivo*, especially for the early stages crucial for therapy outcome. In this context, we examined several *in vivo* contrast agents designed to visualize factors involved in tumor development to explore their potential to recognize early lesions leading to malignant tumors. Preclinical K-ras mouse model of NSCLC developed lung tumors from 1 week of age<sup>20</sup> and enabled tracking of cancer development from early to late stages.

Somewhat contrary to the expectations from other lung tumor models,<sup>27</sup> the contrast agents activated by Cathepsin B and MMPs did not show tumor-specific signals in NSCLC model. Conversely, IntegriSense targeting  $\alpha\beta3$  and  $\alpha\beta5$

integrins shown to be upregulated in tumors and angiogenic cells<sup>6</sup> demonstrated specific accumulation not only in the developed tumors at 4 and 18 weeks, but also in pleural lesions of 2-week-old mice.

Quantitative analysis for IntegriSense fluorescence was done to study diagnostic potential by comparison of fluorescence ratios in lesions/tumors versus background fluorescence in surrounding tissues such as spinal cord, heart, skin as well as lung parenchyma. Adult mice demonstrated enhanced fluorescence; moreover the elevation was observed already at 2 weeks of age, which, if confirmed in humans, could enable early recognition of tumors or premalignant lesions. The main problem of tumor detection at this stage was high IntegriSense accumulation in PBVA. Higher IntegriSense background in the lungs of 2- versus 4- and 18-week-old mice can be explained by still ongoing lung development in 2-week-old mice, which agrees with enhanced  $\alpha\beta3$ -integrin expression in endothelial cells during wound and tumor angiogenesis<sup>34</sup> or inflammation.<sup>35</sup> The PBVA fluorescence was sometimes similar to the level in the lesions, however, was highly variable and did not significantly differ between lungs from WT and K-ras littermates. This point was confirmed by the analysis of the fluorescence in the lesions versus healthy lung parenchyma, which also showed significantly enhanced fluorescence in lesions. Typical localization of pleural lesions in the lung periphery allowed discrimination from major blood vessels and airways, and enabled the lesion detection against lung parenchyma with the smallest cut-off size of 200  $\mu\text{m}$ . It has to be stated though that lack of IntegriSense specificity at this stage together with the information on the peripheral lesion location still enabled the *ex vivo* lesion detection, but was not enough for *in vivo* applications. The contrast versus healthy lung tissue was further significantly enhanced in adult animals creating a solid basis for integrin-targeted imaging as a lung tumor detection tool at later stages of the disease.

The specificity of IntegriSense targeting was confirmed by colocalization with its target,  $\alpha\beta3$ -integrin in the lesions and tumors, but not healthy lung tissue. The enhanced  $\alpha\beta3$ -integrin level versus WT already at 2 weeks and further elevation towards 4 and 18 weeks of age shown by immunofluorescence correlated with macroscopic *ex vivo* fluorescent imaging. The macroscopic evaluation of reliability for IntegriSense-directed tumor detection also showed high capacity of such imaging versus *ex vivo* color appearance. The specificity of the integrin targeting was successfully confirmed for cancer patients. IntegriSense target showed high percent of positive recognition for squamous cell carcinoma and adenocarcinoma (76.4 and 68.9%, respectively, on  $n = 89$  and  $n = 45$  patient biopsies) with no false positives in healthy tissue for 78 patients showing reliable cancer recognition in clinic. The recognition and false positive values were in fact comparable with cancer markers widely accepted as a basis for clinical lung cancer detection.<sup>36</sup> We believe that in combination with such imaging methods as MRI or intraoperative

imaging integrin targeting could be also successfully applied to recognize the lesions on the early cancer stage.

Lesion characterization by immunofluorescence demonstrated that the lesions at 2 weeks differed from further developed tumors at 4 and 18 weeks of age. The lesion cells at 2-week-old mice did not show the degrees of proliferation activity (Ki-67 and EphA2) and disease progression (EGFR)<sup>33,37</sup> typical for later stages, but already started malignant transformation into adenocarcinomas or adenomas, major tumor types in NSCLC.<sup>2</sup>

The analysis of *in vivo* tomography for the lesions/tumors revealed high potential of FMT-XCT diagnostic imaging in preclinical model. The robust and reliable detection of tumors requires the combination of both XCT and FMT channels, which is successfully realized in the imaging system applied in this study. *In vivo* approach could be successfully applied at 4 and 18 weeks of age, but high fluorescence accumulation in PBVA did not allow lesion detection at earlier stage, possibly due to mouse age in this preclinical cancer model.

In this work, we performed pilot experiments, which showcased successful application of  $\alpha v \beta 3$ -integrin targeting for *ex vivo* and *in vivo* lung tumor recognition in preclinical NSCLC model and confirmed its high potential for possible clinical applications. *Ex vivo* detection was successful for lesions/tumors in 2-, 4- and 18-week old animals, the recognition for the 2-week-old mice was, however, complicated by the high agent accumulation in PBVA regions. We also

proved that integrin targeting could detect developing PL before accepted cancer markers can recognize them, which was also additionally confirmed by  $\alpha v \beta 3$  integrin staining at different stages of the disease. To thoroughly demonstrate full potential and utility of the method for monitoring disease progression and response to treatment, further investigations involving longitudinal studies with preclinical models and human patients with suspected lung cancer or lung cancer in the early stages are required. Potential preclinical and clinical implications include the tumor imaging and anticancer therapy monitoring using integrin-targeted agents in lung cancer including NSCLC and mesotheliomas, which would utilize high specificity and predictive value of this agent in early lung cancer and remarkable sensitivity of fluorescence molecular tomography. Further application areas could include intraoperative integrin targeting seriously enhancing the accuracy of tumor detection. The developed integrin targeting agent can be applied as a theranostic probe when coupled with photodynamic therapy agent or as an early lung cancer diagnostic MRI contrast similar to MRI-adapted VEGF targeted probe.<sup>38</sup> Correspondingly, this principle could be ported into diagnostics toward early disease detection.

### Acknowledgements

The authors thank Sarah Glasl, Claudia Mayerhofer and Florian Jurgeleit for the excellent technical assistance. The authors declare no conflict of interests.

### References

- Alberg AJ, Ford JG, Samet JM. Epidemiology of lung cancer: ACCP evidence-based clinical practice guidelines (2nd edition). *Chest* 2007;132:29S–55S.
- Riely GJ, Marks J, Pao W. KRAS mutations in non-small cell lung cancer. *Proc Am Thorac Soc* 2009;6:201–5.
- Bos JL. ras oncogenes in human cancer: a review. *Cancer Res* 1989;49:4682–9.
- de Seranno S, Meuwissen R. Progress and applications of mouse models for human lung cancer. *Eur Respir J* 2010;35:426–43.
- Yilmaz M, Christofori G, Lehembre F. Distinct mechanisms of tumor invasion and metastasis. *Trends Mol Med* 2007;13:535–41.
- Caccavari F, Valdembrì D, Sandri C, et al. Integrin signaling and lung cancer. *Cell Adhes Migr* 2010;4:124–9.
- Guo W, Giancotti FG. Integrin signalling during tumour progression. *Nat Rev Mol Cell Biol* 2004;5:816–26.
- Bublil EM, Yarden Y. The EGF receptor family: spearheading a merger of signaling and therapeutics. *Curr Opin Cell Biol* 2007;19:124–34.
- Brooks PC, Clark RA, Cheresh DA. Requirement of vascular integrin  $\alpha v \beta 3$  for angiogenesis. *Science* 1994;264:569–71.
- Stupp R, Ruegg C. Integrin inhibitors reaching the clinic. *J Clin Oncol* 2007;25:1637–8.
- Friedlander M, Brooks PC, Shaffer RW, et al. Definition of two angiogenic pathways by distinct  $\alpha v$  integrins. *Science* 1995;270:1500–2.
- Danen EH, van Kraats AA, Cornelissen IM, et al. Integrin beta 3 cDNA transfection into a highly metastatic  $\alpha v \beta 3$ -negative human melanoma cell line inhibits invasion and experimental metastasis. *Biochem Biophys Res Commun* 1996;226:75–81.
- Desgrosellier JS, Cheresh DA. Integrins in cancer: biological implications and therapeutic opportunities. *Nat Rev Cancer* 2010;10:9–22.
- Cai W, Wu Y, Chen K, et al. In vitro and in vivo characterization of  $^{64}\text{Cu}$ -labeled Abegrin, a humanized monoclonal antibody against integrin  $\alpha v \beta 3$ . *Cancer Res* 2006;66:9673–81.
- Boles KS, Schmieder AH, Koch AW, et al. MR angiogenesis imaging with Robo4- vs.  $\alpha v \beta 3$ -targeted nanoparticles in a B16/F10 mouse melanoma model. *FASEB J* 2010;24:4262–70.
- Chen X, Liu S, Hou Y, et al. MicroPET imaging of breast cancer  $\alpha v$ -integrin expression with  $^{64}\text{Cu}$ -labeled dimeric RGD peptides. *Mol Imaging Biol* 2004;6:350–9.
- Chen X, Park R, Hou Y, et al. MicroPET imaging of brain tumor angiogenesis with  $^{18}\text{F}$ -labeled PEGylated RGD peptide. *Eur J Nucl Med Mol Imaging* 2004;31:1081–9.
- Haubner R, Weber WA, Beer AJ, et al. Noninvasive visualization of the activated  $\alpha v \beta 3$  integrin in cancer patients by positron emission tomography and [ $^{18}\text{F}$ ]Galacto-RGD. *PLoS Med* 2005;2:e70.
- Fushiki H, Kanoh-Azuma T, Katoh M, et al. Quantification of mouse pulmonary cancer models by microcomputed tomography imaging. *Cancer Sci* 2009;100:1544–9.
- Johnson L, Mercer K, Greenbaum D, et al. Somatic activation of the K-ras oncogene causes early onset lung cancer in mice. *Nature* 2001;410:1111–6.
- Sarantopoulos A, Themelis G, Ntziachristos V. Imaging the bio-distribution of fluorescent probes using multispectral epi-illumination cryoslicing imaging. *Mol Imaging Biol* 2011;13:874–85.
- Ale A, Ermolayev V, Herzog E, et al. FMT-XCT: in vivo animal studies with hybrid fluorescence molecular tomography-X-ray computed tomography. *Nat Methods* 2012;9:615–20.
- Schulz RB, Ale A, Sarantopoulos A, et al. Hybrid system for simultaneous fluorescence and x-ray computed tomography. *IEEE Trans Med Imaging* 2010;29:465–73.
- Soubret A, Ntziachristos V. Fluorescence molecular tomography in the presence of background fluorescence. *Phys Med Biol* 2006;51:3983–4001.
- Soubret A, Ripoll J, Ntziachristos V. Accuracy of fluorescent tomography in the presence of heterogeneities: study of the normalized Born ratio. *IEEE Trans Med Imaging* 2005;24:1377–86.
- Mohajerani P, Koch M, Thurmel K, et al. Fluorescence-aided tomographic imaging of synovitis in the human finger. *Radiology* 2014;272:865–74.
- Niedre MJ, de Kleine RH, Aikawa E, et al. Early photon tomography allows fluorescence detection of lung carcinomas and disease progression in mice in vivo. *Proc Natl Acad Sci USA* 2008;105:19126–31.

28. Qian Q, Wang Q, Zhan P, et al. The role of matrix metalloproteinase 2 on the survival of patients with non-small cell lung cancer: a systematic review with meta-analysis. *Cancer Invest* 2010;28:661–9.
29. Kossodo S, Pickarski M, Lin SA, et al. Dual in vivo quantification of integrin-targeted and protease-activated agents in cancer using fluorescence molecular tomography (FMT). *Mol Imaging Biol* 2010;12:488–99.
30. Abutaily AS, Addis BJ, Roche WR. Immunohistochemistry in the distinction between malignant mesothelioma and pulmonary adenocarcinoma: a critical evaluation of new antibodies. *J Clin Pathol* 2002;55:662–8.
31. Mathieu A, Weynand B, Verbeken E, et al. Comparison of four antibodies for immunohistochemical evaluation of epidermal growth factor receptor expression in non-small cell lung cancer. *Lung Cancer* 2010;69:46–50.
32. Faoro L, Singleton PA, Cervantes GM, et al. EphA2 mutation in lung squamous cell carcinoma promotes increased cell survival, cell invasion, focal adhesions, and mammalian target of rapamycin activation. *J Biol Chem* 2010;285:18575–85.
33. Ito T, Mitui H, Udaka N, et al. Ki-67 (MIB 5) immunostaining of mouse lung tumors induced by 4-nitroquinoline 1-oxide. *Histochem Cell Biol* 1998;110:589–93.
34. Somanath PR, Malinin NL, Byzova TV. Cooperation between integrin alphavbeta3 and VEGFR2 in angiogenesis. *Angiogenesis* 2009;12:177–85.
35. Dingemans AM, van den Boogaart V, Vosse BA, et al. Integrin expression profiling identifies integrin alpha5 and beta1 as prognostic factors in early stage non-small cell lung cancer. *Mol Cancer* 2010;9:152.
36. Travis WD, Brambilla E, Riely GJ. New pathologic classification of lung cancer: relevance for clinical practice and clinical trials. *J Clin Oncol* 2013;31:992–1001.
37. Tong Q, Zheng L, Kang Q, et al. Upregulation of hypoxia-induced mitogenic factor in bacterial lipopolysaccharide-induced acute lung injury. *FEBS Lett* 2006;580:2207–15.
38. Hsieh WJ, Liang CJ, Chieh JJ, et al. In vivo tumor targeting and imaging with anti-vascular endothelial growth factor antibody-conjugated dextran-coated iron oxide nanoparticles. *Int J Nanomed* 2012;7:2833–42.